PAPER

Combining Parallel Adaptive Filtering and Wavelet Threshold Denoising for Photoplethysmography-Based Pulse Rate Monitoring during Intensive Physical Exercise

Chunting WAN[†], *Member*, Dongyi CHEN[†a)], Juan YANG[††], *and* Miao HUANG[†], *Nonmembers*

SUMMARY Real-time pulse rate (PR) monitoring based on photo-plethysmography (PPG) has been drawn much attention in recent years. However, PPG signal detected under movement is easily affected by random noises, especially motion artifacts (MA), affecting the accuracy of PR estimation. In this paper, a parallel method structure is proposed, which effectively combines wavelet threshold denoising with recursive least squares (RLS) adaptive filtering to remove interference signals, and uses spectral peak tracking algorithm to estimate real-time PR. Furthermore, we propose a parallel structure RLS adaptive filtering to increase the amplitude of spectral peak associated with PR for PR estimation. This method is evaluated by using the PPG datasets of the 2015 IEEE Signal Processing Cup. Experimental results on the 12 training datasets during subjects' walking or running show that the average absolute error (AAE) is 1.08 beats per minute (BPM) and standard deviation (SD) is 1.45 BPM. In addition, the AAE of PR on the 10 testing datasets during subjects' fast running accompanied with wrist movements can reach 2.90 BPM. Furthermore, the results indicate that the proposed approach keeps high estimation accuracy of PPG signal even with strong MA.

key words: *photoplethysmography (PPG), pulse rate (PR), motion artifacts (MA), recursive least squares (RLS), wavelet threshold denoising*

1. Introduction

Pulse Rate (PR) is an important indicator reflecting physiological state. The estimation of real-time PR under different conditions is conductive to monitor and analyze the health status of individuals in their daily lives. Besides, PR monitoring can also be utilized to arrange the reasonable exercise intensity [1]. Therefore, real-time, non-invasive and accurate monitoring of PR has attracted much research interest in recent years.

Nowadays, there are mainly two methods used to monitor PR in wearable devices. One is the traditional method based on Electroocardiogram (ECG) signal [2], [3], it requires several electrodes to simultaneously collect physiological signal from different parts of human body, and then PR will be estimated according to the acquired ECG signal. This method is commonly used in clinical scenarios and can

provide high measurement accuracy. However, it is inconvenient to acquire the ECG signal due to the use of several electrodes cling to human body. The second approach proposed in [4], [5] uses photoelectric technology to detect the blood volume changes induced by cardiac diastole and contraction regularly for estimating PR. This approach has advantages of convenient signal acquisition, i.e., only needs a photoelectric PPG sensor cast light on skin [6], and the activities of human body can not be influenced by it. This approach is widely used in wearable monitoring devices, such as smart watches [7], etc.

PPG signal is susceptible to noise especially during movement. The noises are mainly from ambient light, random noises and motion artifacts (MA) particularly. MA is mainly caused by ambient light leaking into the gap between the PPG sensor surface and skin surface [4]. However, subject movement would then invariably disturb the contact between the PPG sensor and the skin, corrupting the PPG signal with MA. PPG signal with noise may degrade the accuracy and reliability of algorithms for estimating PR. Therefore, how to reduce the influence of exercise MA and real-time PR estimation from PPG signal is the difficulty problem we focused on (see Fig. 1). At present, many techniques were proposed to reduce MA from PPG signal during movement, including Wavelet Denoising [8], [9], Independ Component Analysis (ICA) [10], [11], Singular Spectrum Analysis (SSA) [12], [13], Empirical Mode Decomposition (EMD) [14], [15], and [16], Kalman Filtering [17], Adaptive Filtering [18], [19], Particle Filtering [20], [21] and other mixture of methods [22], [23], etc.

Recently, the author of [12] proposed a method called TROIKA, in which SSA has been used to decompose the
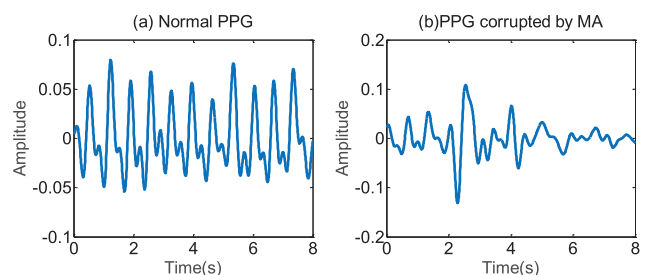
Fig. 1 The PPG signal in time-domain (from subject 4). (a) is good-quality PPG signal. (b) is PPG signal corrupted by MA.

original PPG signal into multiple components, then the tri-axial synchronous acceleration signals are uesd to identify the components related to MA. After removing these components, sparse signal reconstruction was carried out on PPG signal with the remaining components to obtain clean PPG signal. In this method, when the spectral peak position corresponding to the MA is very close to the desired PR peak position, the deviation between the estimated PR and the ground truth PR trajectory will occur.

In order to overcome this weakness, Zhang introduced a method namely JOSS and derived a multiple measurement vector (MMV) model which had been used for joint spectrum estimation [13]. In comparison with TROIKA, the JOSS method provided a lower mean error at the expense of a higher standard deviation. The drawback of JOSS is the using of the intensive m-focuss algorithm for computing the spectrum. Furthermore, the JOSS method evaluates the results by excluding some initial time windows of the dataset.

Sun et al. [14] used the acceleration signals as the spectral subtraction of the reference signal to remove the MA in the PPG signal, and achieved a good PR estimation effect. However, their algorithm used the real heart rate (HR) as reference information. This is unrealistic in real-time monitoring of actual HR, and the practicality of the algorithm is greatly reduced. Galli et al. [17] presented an approach using subspace decomposition denoising algorithm, which decomposed effective component and pseudo-component based on maximum uncorrelated criteria, and finally, the Fourier-based HR estimation would be smoothed and tracked by a Kalman filter. This algorithm can be independent of the initial evaluation of PR and has a certain robustness. However, the algorithm is not suitable for real-time PR evaluation because of the needing to smoothes the result of PR estimation.

Mashhadi et al. [24] firstly extracted the MA component form the tri-axial acceleration signals by SVD transformation, and then used the MA component of the extracted acceleration as the reference signal of cascade adaptive filtering LMS to remove the MA of PPG signal. However, this method may extract multiple MA from tri-axial acceleration signals as reference signal, and thus leading to a large amount of calculation time. Fallet et al. [19] used the normalized least mean square (NLMS) adaptive filtering algorithm on every possible PPG-ACC combination for suppress MA and then selected the optimal one. The complexity grows when the number of combinations increases. In [21], Nathan estimated PR values with the results of conditional posterior probability density estimation by using particle filtering through prediction and updating processes. This algorithm noticeably improves the estimation accuracy by correcting outliers. However, serious errors may be caused when repetitive estimations are performed.

Adaptive filtering is a popular and effective technique for estimating PR from corrupting PPG signal with MA. The advantages of using adaptive method are faster response time and the capability of continuous processing in time-varying condition. However, the limitation of adaptive filter-

ing is that the choice of the reference signal seriously affects the performance of reducing MA.

In this paper, we propose a new parallel method structure combining wavelet threshold denoising with parallel RLS adaptive filtering. The parallel method structure increases the amplitude of spectral peak associated with PR for PR estimation. The parallel RLS adaptive filtering not only solves the problem that only using one of X, Y, Z tri-axial acceleration signals as the reference signal of RLS adaptive filtering cannot completely represent the source of interference signals, but also avoid the induction of additional interference frequency components caused by using synthesizing acceleration signal $\sqrt{X^2 + Y^2 + Z^2}$ as reference signal. Wavelet threshold denoising is a supplement of RLS adaptive filtering to reduce non-motion generated interference. Moreover, a spectral tracking and verifying method is adopted to estimate current PR values considering previous evaluation results. Experiments with training and testing datasets are performed to verify the accuracy of our method.

The remainder of this paper is organized as follows: Sect. 2 introduces the details of PPG signal processing and PR estimation methods. Section 3, the parameter settings of our algorithm are presented. Then the experimental results have been given to evaluate the performance of our proposed method. Conclusion are described in the last section.

2. Methods

Figure 2 shows a flowchart of the proposed method. At the first stage, two channels PPG signals and tri-axial acceleration signals respectively pass through the bandpass filtering for eliminating interferences beyond the frequency range. PPG signal collected from two channels are averaged and normalized to form a composite PPG signal, and tri-axial acceleration signals are normalized separately. Next, the effect of motion artifacts (MA) can be reduced from the composite PPG signal by wavelet threshold denoising and parallel RLS adaptive filtering. In parallel RLS adaptive filtering, the tri-axial acceleration signals for reference are respectively offered into RLS filtering block. At last, the real-time PR values are obtained by evaluating and verifying from logic combination of wavelet threshold denoising
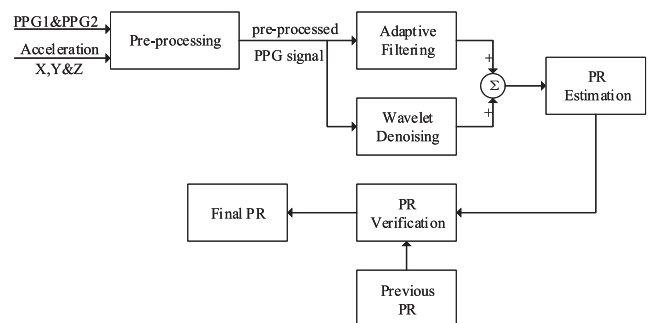

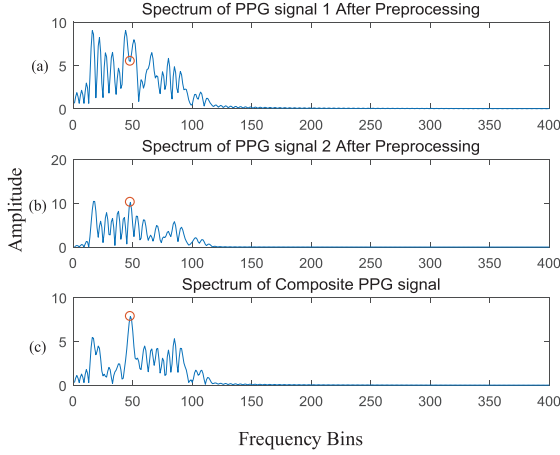**Fig. 2** Flowchart of the proposed method.

Fig. 3 An example showing the effect of pre-processing, and the red circle indicates the spectral peak associated with the ground truth value of PR. (a) Spectrum of PPG signal 1 after pre-processing. (b) Spectrum of PPG signal 2 after pre-processing. (c) Spectrum of composite PPG signal after pre-processing.

and parallel RLS adaptive filtering.

2.1 Pre-Processing

PPG signal obtained from the photoelectric pulse sensor contain underlying PPG signal, random noises and motion artifacts (MA). The range of normal PR value of human in the static or movement state is generally 30–200 BPM/min, hence the corresponding frequency is 30/60–200/60 hz. A bandpass filtering of 0.5–3.5 hz is designed to eliminate the interference signals beyond the frequency range from both PPG signal and acceleration signals. Since two channels PPG datas are acquired from the two close photoelectric pulse sensors, a composite PPG signal is used for estimating PR instead of using them separately. Due to use composite PPG signal, partial random noises may be reduced. In Figs. 3 (a) and (b), the spectrum of PPG1 and PPG2 after pre-processing and being normalized is shown. It is clearly that multiple interference peaks appear in the spectrum of PPG1 and PPG2. It can be seen in Fig. 3 (c) that PR value can be obtained more easily by using composite PPG signal. Since some of the interfering signals are in the same frequency band with the pure PPG signal, a simple bandpass filtering cannot completely eliminate the interference of motion artifacts. In what follows, a parallel method has been proposed.

2.2 Wavelet Threshold Denoising

After pre-processing, the PPG signal still contains part of random noises and strong MA. Wavelet threshold denoising is a common method for removing MA from PPG signal [8], [9]. It can be seen from Fig. 4 that wavelet threshold denoising includes wavelet decomposition, threshold processing and wavelet reconstruction. The procedure of wavelet threshold denoising can be described as follows.

Algorithm 1 Wavelet threshold denoising algorithm

1: **Initialize:**
2: Wavelet decomposition layer *level* ← 7
3: Wavelet basis function *method* ← 'haar'
4: Wavelet coefficients C, the length of wavelet coefficients L
5: Wavelet decomposition $[C, L] ← wavedec(PPG, level, method)$
6: CA_i represents the i–th level approximation coefficients, CD_i represents i level detailed coefficients
7: $CA_7 ← 0, CD_7 ← 0$.
8: **for** i=2:*level*+2 **do**
9: average value $th ← mean(abs(CD_i))$
10: **if** $CD_{ij} > th, \forall j = 1, 2, 3, \ldots$
11:      $CD_{ij} ← th$
12: **else if** $CD_{ij} < -th, \forall j = 1, 2, 3, \ldots$
13:      $CD_{ij} ← -th$
14: **else**
15:      $CD_{ij} ← CD_{ij}$
16: **end if**
17: **end for**
18: Wavelet reconstruction $PPG ← waverec(C, L, method)$
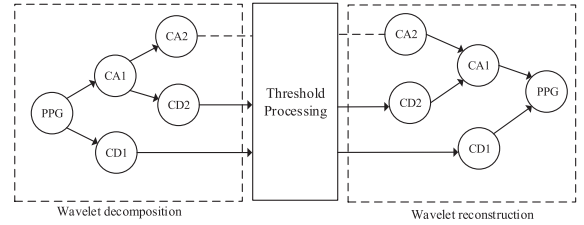19: **return** PPG.

Fig. 4 Block diagram of wavelet threshold denoising.

First, the vector of wavelet coefficients containing important information of PR signal is generated by wavelet decomposition. After wavelet decomposition, the wavelet coefficients of the signal is larger than that of the noises. In the second step, by selecting an appropriate threshold, the wavelet coefficients associated with the noises are suppressed. At last, the denoised signal is achieved by reconstructed using inverse wavelet transform. The choices of appropriate mother wavelet function and a suitable threshold are the key points for achieving the best denoising performance. Haar wavelet function is usually applied in data processing and it is easy to calculate and understand [8]. In this paper, the threshold *th* is selected according to the process of wavelet threshold denoising in algorithm 1.

MA contains a strong non-gaussian component, so using wavelet threshold denoising alone cannot eliminate the effect of MA well. Therefore, the adaptive-filtering-based method has been used and the details of the method will be discussed as follows.

2.3 Parallel RLS Adaptive Filtering

MA has a strong correlation with the human motion, therefore, using the acceleration signals as the reference signal of the adaptive filtering for reducing MA is currently widespread approach. RLS adaptive filtering algorithm is a least-square-criterion-based method, which has the fea-
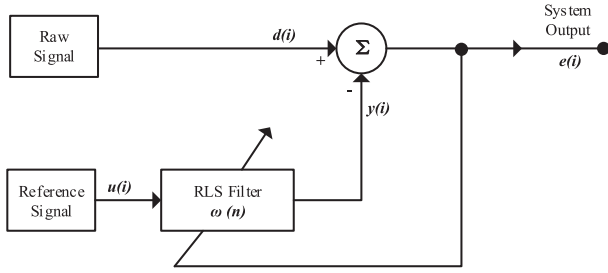
Fig. 5 The block diagram of RLS adaptive filtering system, which has two inputs. One is the desired signal $d(i)$, the other is reference signal $u(i)$. $e(i)$ represents the output signal.

Fig. 6 Block diagram of the parallel RLS adaptive filtering.

tures of fast convergence and stable filtering. The block diagram of RLS adaptive filtering system is shown in Fig. 5. The RLS algorithm differs from the LMS algorithm in that $E\{e^2(n)\}$ is used as the cost function, denoted by $J(n)$ is shown in Eq. (1).

$$
\begin{aligned}
J(n) &= \sum_{i=0}^{n} \lambda^{n-i} |e(i)|^2 \\
&= \sum_{i=0}^{n} \lambda^{n-i} |d(i) - \omega(n)^T u(i)|^2
\end{aligned}
\tag{1}
$$

Where $e(i)$ represents the output error signal, λ is the forgetting factor, $d(i)$ represents the desired output signal, $\omega(n)$ is the FIR filter weight vector, $u(i)$ is the input reference signal, $i = 0, 1, 2, \ldots, n$ denotes sequence length. Take the derivative of weight vector $\omega(n)$ to obtain minimum of the cost function $J(n)$.

$$
\frac{\partial J(n)}{\partial \omega(n)} = 0
\tag{2}
$$

By Eqs. (2) and (1) the optimal weight vector $\omega(n)$ can be written as

$$
\omega_{opt}(n) = R^{-1}(n) * r(n)
\tag{3}
$$

Where $R(n) = \sum_{i=0}^{n} \lambda^{n-i} u(i) u^T(i)$ and $r(n) = \sum_{i=0}^{n} \lambda^{n-i} u(i) d(i)$. The weight vector $\omega(n)$ is updated with N iterations. The process of an iteration has been described as follows.

$$
k(n) = \frac{p(n-1)u(n)}{\lambda + u^T(n)p(n-1)u(n)}
\tag{4}
$$

$$
y(n) = \omega^T(n-1)u(n)
\tag{5}
$$

$$
e(n) = d(n) - y(n)
\tag{6}
$$

$$
\omega(n) = \omega(n-1) + k(n)e(n)
\tag{7}
$$

$$
p(n) = \frac{1}{\lambda}[p(n-1) - k(n)u^T(n)p(n-1)]
\tag{8}
$$

Where n changes from 1 to N. It is necessary to initialize the covariance matrix $P(n)$, forgetting factor λ and filter order N during the iterations [25]. It can be seen from Eq. (7) that the update of weight vector $\omega(n)$ is related to gain vector $k(n)$ and output error signal $e(n)$, where $e(n)$ has been updated by Eq. (6) and $k(n)$ depends on the covariance matrix $p(n)$
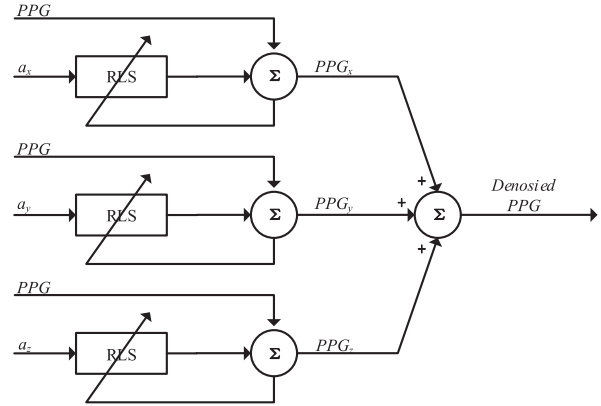
according to Eq. (8).

The selection of appropriate reference signal in the adaptive filter determine the effect of filter. It is should be noted that X, Y, Z tri-axial acceleration signals are taken as the reference signal of RLS adaptive filtering respectively, which cannot completely represent the source of interference signals. The component of acceleration signals which are not related to interference signals is introduced by synthesizing acceleration signal $\sqrt{X^2 + Y^2 + Z^2}$ as reference signal. In this paper, for the purpose of reducing MA and estimating PR, a parallel filtering structure is proposed by using RLS adaptive filtering in Fig. 6. The method can increase the amplitude of spectral peak associated with PR for PR estimation. X, Y, Z tri-axial acceleration signals are denoted by a_x, a_y, a_z as reference signal enter the RLS adaptive filtering respectively, the output denoised PPG signal is denoted by PPG can be obtain by Eq. (9).

$$
PPG = PPG_x + PPG_y + PPG_z
\tag{9}
$$

Where PPG_x, PPG_y and PPG_z represent the output of each RLS block respectively.

In most of the cases, the parallel RLS adaptive filtering method proposed in this paper can reduce MA. However, MA is not completely caused by the acceleration signals. Therefore the propose method structure that combines wavelet threshold denoising with parallel RLS adaptive filtering to provide a more appropriate signal for PR estimation. Figure 7 (a) shows the spectrum of PPG signal after wavelet threshold denoising, and the red circle indicates the spectral peak associated with the ground truth value of PR. After wavelet threshold denoising, two strong spectral peaks appear, and the ground truth value of PR is not at the highest spectral peak. It can be observed from Fig. 7 (b) that multiple spectral peaks appear in the spectrum after the PPG signal passing through the parallel RLS adaptive filtering. Figure 7 (c) is the spectrum of the PPG signal using the method we proposed. We can see that the spectral peak can be easily tracked to estimate PR value.
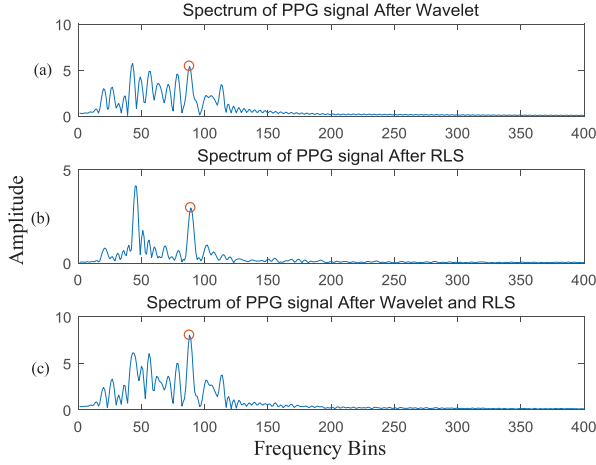
Fig. 7 An example showing the result after removing MA, and the red circle indicates the spectral peak associated with the ground truth value of PR. (a) Spectrum of PPG signal after wavelet threshold denoising. (b) Spectrum of PPG signal after the parallel RLS adaptive filtering. (c) Spectrum of parallel PPG signal after wavelet threshold denoising and RLS adaptive filtering.

2.4 PR Estimation

PPG signal after processing by parallel eliminating MA method may cause superposition of interfering signals, so it is difficult to directly estimate the value of PR in the time domain. Therefore, we estimate the PR value from PPG spectrum, which is acquired by Fast Fourier Transform (FFT). The estimation of PR consists of initial estimation of PR, spectral peak selection and spectral peak verification.

For initial estimation of PR, since there were no previous PR values as references, subjects are required to reduce their hand movements in the first few seconds in the datasets for avoiding the influence of MA [12]. After FFT, the location corresponding to the highest spectral peak is selected to estimate PR value in this stage. Due to the PR value of human body does not change a lot in two successive time windows [12], [13], we can determine the search range of current spectral peak location by the location of pervious time window. According to the location of the spectral peak N_p obtained in the last time window, the current location range of the spectral peak is considered as $R_0 = [N_p − \epsilon, N_p + \epsilon]$, where ϵ is a little positive integer. The process of spectral peak selection is divided into the following steps.

*Step*1 : The maximum of amplitude spectral peak is selected in the spectrogram and its maximum amplitude value *Pmax* is recorded. The spectral peaks amplitude value greater than $0.5 * Pmax$ are selected as the candidate spectral peak.

*Step*2 : The locations of the spectral peaks without in the range R_0 are removed, the 2nd and 3rd largest spectral peaks are selected as candidate spectral peaks within the scope meeting the requirements. The locations of these spectral peaks are denoted by N_i ($i = 1, 2, 3$).

*Step*3 : Denote by N_c the location of PR estimated in the current time window. The spectral peak amplitude value with

the location N_i is compared with that of N_p successively. N_i will be selected as the location of current spectral peak N_c when the condition $N_i − N_p \leq \delta$ is satisfied at the first time. If the spectral peak satisfying the conditions can not be found, we set $N_c = N_p$.

$$BPM_{cur} = \frac{N_c * 60 * F_s}{N_{fft}} \tag{10}$$

After determining N_c, the current estimation of PR value BPM_{cur} is obtained according to Eq. (10), where F_s is the sampling rate of the PPG signal and N_{fft} is the number of points for FFT. Due to 2s' overlap between the current time window and the last time window, there is a certain relationship between the current and the last PR value, and the current estimated PR value can be obtained from Eq. (11).

$$BPM_{cur} = \alpha BPM_{cur} + \beta BPM_{-1} + \gamma BPM_{-2} \tag{11}$$

Where $\alpha + \beta + \gamma = 1$, BPM_{-1} and BPM_{-2} represent the results of the previous two estimated PR values. In order to prevent the estimation result of PR value a large change in two successive time windows, the final estimation result of PR value is verified by Eq. (12).

$$BPM_{est} = \begin{cases} BPM_{prev} + \tau, & if \; BPM_{cur} − BPM_{prev} \geq \tau \\ BPM_{prev} − \tau, & if \; BPM_{cur} − BPM_{prev} \leq −\tau \\ BPM_{cur}, & otherwise \end{cases}$$

$$\tag{12}$$

Where τ represents the limit value between the twice estimation, which can be obtained by experience. Denote by BPM_{prev} the estimation of PR in the previous time window.

3. Results

3.1 Datasets

The proposed method was evaluated on the PPG datasets used in 2015 IEEE Signal Processing Cup. The datasets were composed of 12 training and 10 testing recordings and were made available by the authors of Zhang [12]. Each dataset contained two-channel PPG signals, tri-axial acceleration signals, and one-channel ECG signal, recorded simultaneously from a subject. For each subject, the two-channel PPG signals were recorded from wrist by two pulse oximeters with green LEDs (wavelength: 515nm). The acceleration signals were also recorded from wrist by a tri-axial accelerator. The ECG signal was recorded simultaneously from the chest using ECG sensors. All signals were acquired at a sampling frequency 125 Hz.

During 12 training datasets recording, each subject walked or ran on a treadmill with changing speeds in order: the speed of 1–2 km/h for 0.5 min, the speed of 6–8 km/h for 1 min, the speed of 12–15 km/h for 1 min, the speed of 6–8 km/h for 1 min, the speed of 12–15 km/h for 1 min, and the speed of 1–2 km/h for 0.5 min. The 10 testing datasets were recorded when subjects were asked to purposely use

the hand with the wristband to pull clothes, wipe sweat on forehead, and push buttons on the treadmill, in addition to freely swing. The large amplitude of these actions leads to much stronger MA than in the training datasets.

3.2 Parameter Settings

The estimation of PR is performed on a time window of 8 s with a step of 2s interval. An RLS adaptive filtering of order $N = 32$ is used for MA cancellation with the forgetting factor $\lambda = 0.999$ [26]. In estimation of PR stage, the number of points for FFT is chosen to $N_{fft} = 4096$, ϵ and δ are set to 12 and 8. Due to the current estimation of PR overlaps with the previously estimated PR for 2 s, considering that the current estimate PR is the main weight, the parameters α, β and γ are selected as 0.90, 0.05 and 0.05. It can be seen from the ground truth PR vaules that the changes in the adjacent time window are less than 4 BPM. With these considerations in mind, the τ in the Eq. (11) is chosen as 4.

3.3 Performance Evaluation

This paper evaluates the performance of method from the following four indexes, where the ground truth PR value $BPM_{true}(i)$ in each time window is extracted from the simultaneous ECG signal. Denoted by $BPM_{est}(i)$ the estimated PR value in the i–th time window using our proposed algorithm, where W is the total number of time windows. The average absolute error is defined as

$$AAE = \frac{1}{W} \sum_{i=1}^{W} |BPM_{est}(i) - BPM_{true}(i)| \tag{13}$$

The average absolute error percentage is defined as follows:

$$AEP = \frac{1}{W} \sum_{i=1}^{W} \frac{|BPM_{est}(i) - BPM_{true}(i)|}{BPM_{true}(i)} \tag{14}$$

The Bland-Altman plot is also another evaluation index which is used to obtain the difference between the ground truth of PR and estimation of PR values. We also calculate the limit of agreement (LOA) which is defined as $[\mu - 1.96\sigma, \mu + 1.96\sigma]$, where μ denotes the average of the difference and σ represents the standard deviation. Pearson correlation between ground truth and estimation of PR values is also adopted to evaluate the performance of method.

3.4 Results Analysis

The average absolute error (AAE) obtained from all 12 subjects using the RLS adaptive filtering method is listed in Table 1. It can be seen from Table 1 that under the same pre-processing and PR estimation algorithm, the parallel RLS adaptive filtering algorithm proposed in this paper has fewer errors in AAE indexes compared with the cascade RLS adaptive filtering algorithm and the RLS adaptive filtering algorithm which respectively take a_x, a_y, a_z and synthesizing acceleration signals $\sqrt{a_x^2 + a_y^2 + a_z^2}$ as reference signal [28].

Tables 2 and 3 list the AAE and AEP on the 12 Training Datasets across various algorithms in the literature and our proposed algorithm. It is observed that the performance of our proposed method is better than that of other algorithms in most of subjects. The AAE of these subjects are slightly higher but within the acceptable limit. However, the mean AAE and AEP over all 12 subjects of our proposed method are 1.08 ± 1.45 BPM (Mean ± SD) and 1.82% in Tables 2 and 3, which is found the lowest AAE and AEP among

Table 1 Comparison of AAE in BPM under different reference signal and algorithm structures used the same pre-processing and PR estimation algorithm.
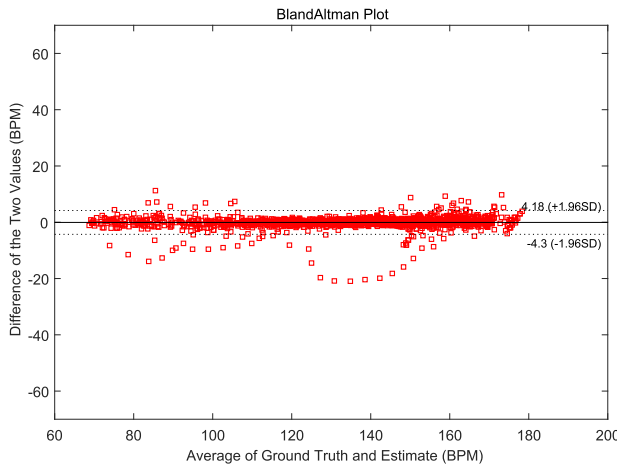
Subject #	1	2	3	4	5	6	7	8	9	10	11	12	Mean ± SD
a_x	1.19	1.55	1.36	1.36	0.82	1.70	3.88	1.08	0.72	3.38	1.00	0.79	1.57 ± 2.44
a_y	1.39	2.15	1.50	1.41	0.86	1.40	1.41	1.00	0.76	3.39	1.20	1.04	1.46 ± 1.93
a_z	1.66	1.89	0.71	1.55	0.74	1.38	0.96	0.77	0.69	4.05	1.17	1.01	1.37 ± 1.72
$\sqrt{a_x^2 + a_y^2 + a_z^2}$	1.70	26.50	0.68	1.28	0.74	9.51	0.91	0.82	0.67	4.93	1.33	2.90	4.33 ± 4.78
Cascaded RLS	1.50	1.48	1.32	2.06	1.25	1.84	1.99	1.02	0.63	3.53	1.37	1.22	1.60 ± 2.56
Parallel RLS	1.08	1.47	1.09	1.24	0.72	1.08	0.90	0.77	0.54	3.30	0.97	0.73	1.16 ± 1.63

Table 2 Comparison of AAE in BPM on the 12 training datasets across various algorithms in the literature.

Subject #	1	2	3	4	5	6	7	8	9	10	11	12	Mean ± SD
TROIKA [12]	2.29	2.19	2.00	2.15	2.01	2.76	1.67	1.93	1.86	4.70	1.72	2.84	2.34 ± 2.47
JOSS [13]	1.33	1.75	1.47	1.48	0.69	1.32	0.71	0.56	0.49	3.81	0.78	1.04	1.28 ± 2.61
SPECTRAP (offline) [16]	1.18	2.42	0.86	1.38	0.92	1.37	1.53	0.64	0.60	3.65	0.92	1.25	1.50 ± 1.95
NOANc [19]	1.75	1.94	1.17	1.67	0.95	1.22	0.91	1.17	0.87	2.95	1.15	1.00	1.40 ± 0.60
SPECMAR [27]	1.22	1.51	0.75	1.26	0.75	1.87	0.80	1.07	0.65	2.24	1.39	1.09	1.21 ± 1.75
Particle Filter [21]	1.91	1.30	1.08	1.63	1.06	1.64	1.09	1.25	1.10	3.41	1.65	1.59	1.56 ± 1.73
SSA+KS [17]	2.72	3.25	1.40	1.21	0.93	2.12	1.40	1.16	1.17	4.14	1.38	1.29	1.85 ± 1.00
Ours	1.11	1.23	0.64	1.26	0.71	1.10	0.85	0.78	0.55	2.85	0.99	0.85	1.08 ± 1.45

Table 3　Comparison of AEP in BPM on the 12 training datasets across various algorithms in the literature.

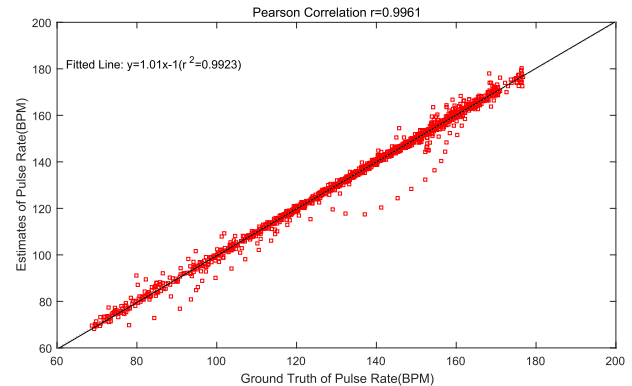| Subject #	1	2	3	4	5	6	7	8	9	10	11	12	Mean
TROIKA [12]	2.18%	2.37%	1.50%	2.10%	1.22%	2.51%	1.27%	1.47%	1.28%	2.49%	1.29%	2.30%	1.82%
JOSS [13]	1.19%	1.66%	1.27%	1.41%	0.51%	1.09%	0.54%	0.47%	0.41%	2.43%	0.51%	0.81%	1.01%
SPECTRAP (offline) [16]	1.04%	2.33%	0.66%	1.31%	0.74%	1.14%	1.36%	0.55%	0.52%	2.27%	0.65%	1.02%	1.12%
NOANc [19]	1.59%	1.99%	1.02%	1.51%	0.75%	1.05%	0.72%	1.04%	0.76%	1.93%	0.79%	0.79%	1.16%
SSA+KS [17]	2.11%	3.02%	1.11%	1.04%	0.70%	1.82%	1.04%	0.97%	0.95%	2.79%	0.91%	0.92%	1.45%
Ours	0.92%	1.20%	0.52%	1.18%	0.55%	0.87%	0.63%	0.68%	0.46%	1.85%	0.65%	0.62%	0.84%

Fig. 8　The Bland-Altman plot of the estimation results on the 12 training datasets, where X-axial represents the average value of the ground truth PR values and the estimated PR values of our proposed algorithm, and the Y-axial represents the error between ground truth PR values and the estimated PR values. The LOA is [−4.30, 4.18] BPM.

Table 4　Comparison of Pearson correlation (PC), limit of agreement (LOA), and runtime of each window on the 12 training datasets across various algorithms in the literature.

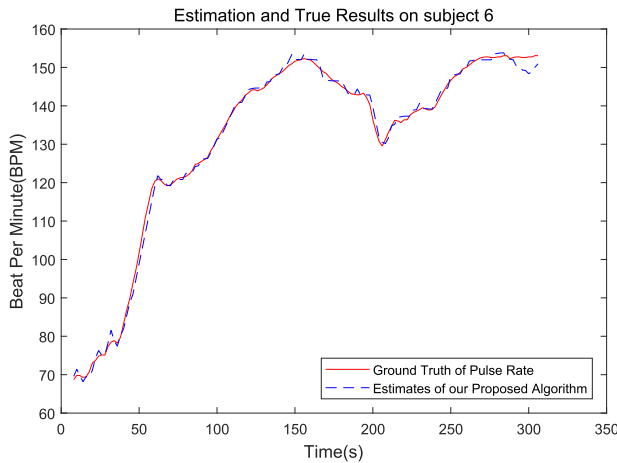| Method	PC (r)	LOA	Runtime
TROIKA [12]	0.992	[−7.26, 4.79]	941.9ms
JOSS [13]	0.993	[−5.94, 5.41]	600ms
SPECTRAP (offline) [16]	0.995	[−5.59, 6.01]	16.2ms
NOANc [19]	–	[−4.71, 4.67]	–
SPECMAR [27]	0.9952	[−4.78, 4.86]	20ms
Particle Filter [21]	–	[−4.75, 4.45]	–
SSA+KS [17]	–	–	1600ms
Ours	0.9961	[−4.30, 4.18]	35ms

Fig. 9　Scatter plot between the ground truth PR values and the estimates of our proposed algorithm over the 12 training datasets. The fitted line is $y = 1.01x − 1$, where x indicates the ground truth PR value, and y represents the estimates our proposed algorithm. The Pearson correlation r is 0.9961.

all algorithm. In contrast, the AAE of TROIKA is 2.34 ± 2.47 BPM, the AEP is 1.82%. For the JOSS algorithm, the AAE is 1.28 ± 2.61 BPM, the AEP is 1.01%. It means that our proposed method can estimate PR more accurately than TROIKA by 53.8% and JOSS by 15.6%. It is found that the overall performance of the proposed algorithm in this paper is better than TROIKA, JOSS, SPECTRAP and other excellent algorithms in the recent three years.

The Bland-Altman plot is given to test agreement between the ground-truth PR values and the estimation PR values. In Fig. 8, the more PR values within the limit of agreement (LOA) area defined by two black dotted lines, the better the consistency between the ground truth and the estimation PR values [12]. In Table 4, the LOA of our algorithm is [−4.30, 4.18] BPM, and 95% of difference values are within this confidence interval, which indicates that the ground truth and estimation of PR values are in good consistency. The Scatter plot objectively measures the fitting degree between the estimated and the ground truth PR values [27]. It is observed from the Fig. 9 that an approximated linear relation exists between ground truth and estimated PR and the linear curve passes close to the origin. The Pearson Correlation r is 0.996. As it is almost nearly 1, it indicates a high correlation between ground truth and estimated PR and the validation of highly accurate estimation of PR. It can be seen from Table 4 that compared with the LOA and Pearson

Correlation values of other algorithms, our algorithm has certain advantages in these two evaluation indicators.

Figure 10 depicts an example of the estimated and the ground truth PR values on recording of subject 6 (randomly chosen). The PR values estimated by the algorithm in this paper almost coincides with the ground truth value of PR, which further illustrates the good performance of the proposed algorithm. The processing time of our algorithm is about 35ms for each window which is computed by using Matlab2017a on four intel cores 3.6GHz processor with 16GB RAM. From Table 4 we can see that our method costs less time compared with the algorithms respectively proposed in Refs. [12], [13], and [17]. It also costs approximate time to the spectral subtraction [16] and [27], which have been recognized as the fastest method. The less computation time costs, the easier it is to integrate the algorithm into

Table 5 Comparison of AAE in BPM on the 10 testing datasets across various algorithms in the literature.

Subject #	1	2	3	4	5	6	7	8	9	10	Mean ± SD
TROIKA [12]	6.63	1.94	1.35	7.82	2.46	1.73	3.33	3.41	2.68	0.51	3.19 ± 2.32
JOSS [13]	8.07	1.61	3.10	7.00	2.99	1.67	2.80	1.88	0.92	0.49	3.05 ± 3.35
SPECTRAP (offline) [16]	4.89	1.58	0.86	1.83	3.05	1.62	1.24	2.04	2.49	1.16	2.13 ± 1.21
NOANc [19]	12.12	4.02	2.52	5.64	3.31	3.39	3.45	5.86	1.56	0.95	4.28 ± 3.16
SPECMAR [27]	6.57	1.76	2.28	2.77	2.94	4.80	2.72	3.28	1.55	0.82	2.95 ± 4.48
SSA+KS [17]	7.91	3.65	3.90	2.44	2.14	2.60	1.86	0.85	3.06	3.38	3.18 ± 1.89
Ours	9.87	1.64	1.76	2.74	2.54	3.42	1.96	3.34	1.02	0.71	2.90 ± 2.28

Fig. 10 The ground truth and estimation results of PR on recordings of subject 6 of the 12 training PPG datasets.

the wearable devices. To further verify the performance of the proposed algorithm, the algorithm is applied to 10 testing datasets, which contain more actions of people in daily life. It is found from the results in Table 5 that the proposed method also shows good performance on AAE compared with the commonly used online algorithm.

4. Conclusion

In this paper, an efficient method combining wavelet threshold denoising with parallel RLS adaptive filtering is proposed to estimate PR values under different motions. It is found that instead of using cascaded RLS adaptive filtering or a single RLS adaptive filtering, a parallel RLS adaptive filtering can provide better performance for the estimation of PR. The performance of the proposed method has been proved by the experiments and the results. Our method can also be used to reduce MA from other physiological signals, such as extracting heart rate from ECG signals during intensive physical exercise. The lower estimation error and less computation time makes our method an ideal choice to be implemented in the wearable devices. Of course, our method also needs to be improved. In Tables 2 and 5, PPG signal is affected by strong MA on some subjects, then the AAE of these subjects is relatively a little higher. This may be since that the MA is not completely related to acceleration signal, but also affected by the pressure, skin color and blood flow [4]. In the future work, the proposed method can

be further optimized. We will investigate that different parameters are used as the reference signals of our algorithm to reduce MA. Considering that this algorithm can be used in wearable devices, the computational complexity of the algorithm can be reduced by using fast RLS adaptive filtering algorithm.

Acknowledgments

References

[1] G.E. Prinsloo, H.G.L. Rauch, and W.E. Derman, "A brief review and clinical application of heart rate variability biofeedback in sports, exercise, and rehabilitation medicine," Phys. Sportsmed., vol.42, no.2, pp.88–99, 2014.

[2] N. Selvaraj, A. Jaryal, J. Santhosh, K.K. Deepak, and S. Anand, "Assessment of heart rate variability derived from finger-tip photoplethysmography as compared to electrocardiography," Journal of Medical Engineering & Technology, vol.32, no.6, pp.479–484, 2009.

[3] S. Izumi, M. Nakano, K. Yamashita, Y. Nakai, H. Kawaguchi, and M. Yoshimoto, "Noise tolerant heart rate extraction algorithm using short-term autocorrelation for wearable healthcare systems," IEICE Trans. Inf. & Syst., vol.E98-D, no.5, pp.1095–1103, May 2015.

[4] J. Allen, "Photoplethysmography and its application in clinical physiological measurement," Physiological Measurement, vol.28, no.3, pp.R1–R39, 2007.

[5] T. Tamura, Y. Maeda, M. Sekine, and M. Yoshida, "Wearable photoplethysmographic sensors—Past and present," Electronics, vol.3, no.2, pp.282–302, 2014.

[6] A.A.R. Kamal, J.B. Harness, G. Irving, and A.J. Mearns, "Skin photoplethysmography—A review," Comput. Methods Programs Biomed., vol.28, no.4, pp.257–269, 1989.

[7] R. Yousefi, M. Nourani, S. Ostadabbas, and I. Panahi, "A motion-tolerant adaptive algorithm for wearable photoplethysmographic biosensors," IEEE J. Biomed. Health Inform., vol.18, no.2, pp.670–681, 2014.

[8] J.Y.A. Foo, "Comparison of wavelet transformation and adaptive filtering in restoring artefact-induced time-related measurement," Biomedical Signal Processing and Control, vol.1, no.1, pp.93–98, 2006.

[9] M. Raghuram, K.V. Madhav, E.H. Krishna, and K.A. Reddy, "Evaluation of wavelets for reduction of motion artifacts in photoplethysmographic signals," 10th International Conference on Information Science, Signal Processing and Their Applications, pp.460–463, 2010.

[10] B.S. Kim and S.K. Yoo, "Motion artifact reduction in photoplethysmography using independent component analysis," IEEE Trans.

Biomed. Eng., vol.53, no.3, pp.566–568, 2006.

[11] R. Krishnan, B. Natarajan, and S. Warren, "Two-stage approach for detection and reduction of motion artifacts in photoplethysmographic data," IEEE Trans. Biomed. Eng., vol.57, no.8, pp.1867–1876, 2010.

[12] Z. Zhang, Z. Pi, and B. Liu, "TROIKA: A general framework for heart rate monitoring using wrist-type photoplethysmographic signals during intensive physical exercise," IEEE Trans. Biomed. Eng., vol.62, no.2, pp.522–531, 2015.

[13] Z. Zhang, "Photoplethysmography-based heart rate monitoring in physical activities via joint sparse spectrum reconstruction," IEEE Trans. Biomed. Eng., vol.62, no.8, pp.1902–1910, 2015.

[14] X. Sun, P. Yang, Y. Li, Z. Gao, and Y.-T. Zhang, "Robust heart beat detection from photoplethysmography interlaced with motion artifacts based on empirical mode decomposition," IEEE-EMBS International Conference on Biomedical and Health Informatics, pp.775–778, 2012.

[15] E. Khan, F.A. Hossain, S.Z. Uddin, S.K. Alam, and M.M. Hasan, "A robust heart rate monitoring scheme using photoplethysmographic signals corrupted by intense motion artifacts," IEEE Trans. Biomed. Eng., vol.63, no.3, pp.550–562, 2016.

[16] B. Sun and Z. Zhang, "Photoplethysmography-based heart rate monitoring using asymmetric least squares spectrum subtraction and Bayesian decision theory," IEEE Sensors J., vol.15, no.12, pp.7161–7168, 2015.

[17] A. Galli, C. Narduzzi, and G. Giorgi, "Measuring heart rate during physical exercise by subspace decomposition and Kalman smoothing," IEEE Trans. Instrum. Meas., vol.67, no.5, pp.1102–1110, 2018.

[18] M.R. Ram, K.V. Madhav, E.H. Krishna, N.R. Komalla, and K.A. Reddy, "A novel approach for motion artifact reduction in PPG signals based on AS-LMS adaptive filter," IEEE Trans. Instrum. Meas., vol.61, no.5, pp.1445–1457, 2012.

[19] S. Fallet and J.-M. Vesin, "Robust heart rate estimation using wrist-type photoplethysmographic signals during physical exercise: An approach based on adaptive filtering," Physiological Measurement, vol.38, no.2, pp.155–170, 2017.

[20] Y. Fujita, M. Hiromoto, and T. Sato, "PARHELIA: Particle filter-based heart rate estimation from photoplethysmographic signals during physical exercise," IEEE Trans. Biomed. Eng., vol.65, no.1, pp.189–198, 2018.

[21] V. Nathan and R. Jafari, "Particle filtering and sensor fusion for robust heart rate monitoring using wearable sensors," IEEE J. Biomed. Health Inform., vol.22, no.6, pp.1834–1846, 2018.

[22] Y. Ye, Y. Cheng, W. He, M. Hou, and Z. Zhang, "Combining nonlinear adaptive filtering and signal decomposition for motion artifact removal in wearable photoplethysmography," IEEE Sensors J., vol.16, no.19, pp.7133–7141, 2016.

[23] M.T. Islam, I. Zabir, S.T. Ahamed, M.T. Yasar, C. Shahnaz, and S.A. Fattah, "A time-frequency domain approach of heart rate estimation from photoplethysmographic (PPG) signal," Biomedical Signal Processing and Control, vol.36, pp.146–154, 2017.

[24] M.B. Mashhadi, E. Asadi, M. Eskandari, S. Kiani, and F. Marvasti, "Heart rate tracking using wrist-type photoplethysmographic (PPG) signals during physical exercise with simultaneous accelerometry," IEEE Signal Process. Lett., vol.23, no.2, pp.227–231, 2016.

[25] S. Haykin, Adaptive Filter Theory, Pearson Education India, 2008.

[26] S.S. Chowdhury, R. Hyder, M.S.B. Hafiz, and M.A. Haque, "Real-time robust heart rate estimation from wrist-type PPG signals using multiple reference adaptive noise cancellation," IEEE J. Biomed. Health Inform., vol.22, no.2, pp.450–459, 2018.

[27] M.T. Islam, S.T. Ahmed, C. Shahnaz, and S.A. Fattah, "SPECMAR: Fast heart rate estimation from PPG signal using a modified spectral subtraction scheme with composite motion artifacts reference generation," Medical & Biological Engineering & Computing, vol.57, no.3, pp.689–702, 2019.

[28] M.R. Ram, K.V. Madhav, E.H. Krishna, K.N. Reddy, and K.A.

Reddy, "Adaptive reduction of motion artifacts from PPG signals using a synthetic noise reference signal," 2010 IEEE EMBS Conference on Biomedical Engineering and Sciences (IECBES), pp.315–319, 2010.

Chunting Wan received the B.S. and M.S. degrees in Measurement and Control from Guilin University of Electronic Technology in 2011 and 2014, respectively. He is currently a Ph.D. student at the University of Electronic Science and Technology of China. His current research interests include wearable computing and affective computing.

Dongyi Chen received the M.S. and Ph.D. degrees in computer and automation, and electronic information engineering from Chongqing University in 1985 and 1997, respectively. He is a professor at the School of Automation Engineering, University of Electronic Science and Technology of China. His post-doctoral research was at the Department of Electrical and Computer Engineering from University of Toronto during 1997–1999. He was a visiting professor at the School of Computing at the Georgia Institute of Technology during 2002–2005. His research interests include augmented reality, wearable computing, and wireless sensor networks.

Juan Yang received the Bachelor degree in Communication and Information system from Guilin University of Electronic Technology in 2015. Since July 2015, she has been a lecturer at the Guilin University of Aerospace Technology. Her research interests include network coding, information theory.

Miao Huang received the B.S. degrees in Internet of Things from Hefei University of Technology in 2017. She is currently a graduate student at the University of Electronic Science and Technology of China. Her current research interests include wearable computing and signal processing.